RSC Advances

PAPER

View Article Online
View Journal | View Issue

Cite this: *RSC Adv.*, 2020, **10**, 27697

Synthesis of bismuth nanoparticle-loaded cobalt ferrite for electrochemical detection of heavy metal ions

Ying He, Zihan Wang, Li Ma, Liya Zhou, Yanjun Jiang* and Jing Gao*

Received 18th March 2020
Accepted 15th July 2020

DOI: 10.1039/d0ra02522d

rsc.li/rsc-advances

As an efficient modified electrode material for the detection of heavy metal ions, bismuth nanoparticles (BiNPs) were loaded on cobalt ferrite ($CoFe_2O_4$), a unique magnetic photocatalytic material, to fabricate a highly sensitive sensor. The obtained BiNPs@$CoFe_2O_4$ nanocomposites showed excellent adsorption and electrical conductivity using a Square Wave Anodic Stripping Voltammetry (SWASV) detection method. Under optimized conditions, the BiNPs@$CoFe_2O_4$/GCE sensor could simultaneously determine Pb^{2+} and Cd^{2+}, with detection limits of 7.3 and 8.2 nM, respectively. In addition, the BiNPs@$CoFe_2O_4$ exhibited acceptable reproducibility and good stability, which indicated great potential for the detection of heavy metal ions in reality.

1. Introduction

Heavy metal ions (HMI) are one of the micro-pollutants that severely affect the environment. Lead (Pb), cadmium (Cd), mercury (Hg), chromium (Cr) and arsenic (As) are highly toxic among the HMIs. These harmful HMIs can cause various diseases of the human body even at low concentration. While not being biodegradable, HMIs can exist in organisms and plants for decades or even hundreds of years after being released into the environment.[1–3] There are several analytical methods for detecting HMIs such as inductively coupled plasma mass spectrometry (ICP-MS), atomic absorption spectroscopy (AAS), X-ray fluorescence spectroscopy (XRF) and inductively coupled plasma optical emission spectroscopy (ICP-OES).[4] However, these technical devices are very expensive and require trained personnel to operate, which limits the application of these methods. Therefore, it is of crucial importance to develop fast, accurate and reliable techniques to detect HMIs for environmental and health protection. Compared to other spectroscopic and optical techniques, electrochemical detection techniques for HMIs have advantages of high sensitivity, low cost and providing on-site and real time monitoring.[5] The modification of electrode can improve electrochemical detection sensitivity and detection limit. Due to the toxicity of mercury, bismuth-based electrodes with low toxicity have been an effective alternative to mercury-based electrodes.[6] The bismuth-based electrodes are environmental friendly and show excellent resolution of neighboring peaks. $CoFe_2O_4$ is a composite oxide containing trivalent iron oxide as the main component, and has attracted much attention in recent years. Compared to other magnetic materials, cobalt ferrite exhibits unique physical, chemical, magnetic and catalytic properties, thus suitable to serve as the substrate to immobilize BiNPs.[7]

In this study, BiNPs@$CoFe_2O_4$ nanocomposites were synthesized by *in situ* reduction method. The nanocomposites were characterized by SEM, TEM, XRD, XPS, and the elemental composition was analyzed by EDS spectrum analysis. After characterizing the synthesized BiNPs@$CoFe_2O_4$ nanocomposites, we modified the glassy carbon electrode (GCE) as an electrochemical sensing platform for the determination of HMIs. Afterwards, the application of the electrochemical sensor in the determination of Pb^{2+} and Cd^{2+} ions in water samples was demonstrated by SWASV technique, and its sensitivity, selectivity, reproducibility and stability were studied. The experimental results showed that the BiNPs@$CoFe_2O_4$ nanocomposite modified sensor has high electrochemical performance and adsorption performance for Pb^{2+} and Cd^{2+} ions.

2. Experimental section

2.1 Materials

$Fe(NO_3)_3 \cdot 9H_2O$, cobalt acetate tetrahydrate, NH_4F, $Bi(NO_3)_3$, $Pb(NO_3)_2$, $CdCl_2$, $MgCl_2$, $FeCl_3$, $CoCl_2$, $ZnCl_2$, $MnCl_2$, $CuSO_4$, $Al(NO_3)_3$, $Ni(NO_3)_2$, H_2SO_4, HNO_3, $C_6H_5Na_3O_7$, $NaBH_4$, CH_3COOH, urea, chitosan (CS), absolute ethanol and ethylene glycol were purchased from Fengchuan Chemical Reagent Co. Ltd. (Tianjin, China), which were all of analytical grade. 0.1 M acetate buffer solution with different pH was used as the supporting electrolyte in this work, which was prepared by mixing stock solutions of 0.1 M sodium acetate and acetic acid.

School of Chemical Engineering and Technology, Hebei University of Technology, 8 Guangrong Road, Hongqiao District, Tianjin, 300130, P. R. China. E-mail: yanjunjiang@hebut.edu.cn; jgao@hebut.edu.cn; Fax: +86-22-60204294; Tel: +86-22-60204945

2.2 Preparation of $CoFe_2O_4$

8 mM ferric nitrate nonahydrate [$Fe(NO_3)_3 \cdot 9H_2O$], 4 mM cobalt acetate tetrahydrate, 80 mM ammonium fluoride (NH_4F) and 120 mM urea were dissolved in 30 mL ultra-pure water, stirred at room temperature for 10 min, and then dripped 0.1 M HNO_3 to the solution pH of 5.0. It was then transferred to a 50 mL polytetra liner. Sealed in autoclave and reacted at 180 °C for 20 h. The sediment was collected after cooling naturally to room temperature, and finally washed three times with deionized water and ethanol. The final product (cobalt ferrite porous microspheres, $CoFe_2O_4$) was obtained after drying at 60 °C for 6 h.[8]

2.3 Preparation of BiNPs@$CoFe_2O_4$ nanocomposites

Certain amount of $CoFe_2O_4$ was dispersed in 5 mL of ethylene glycol and ultrasonicated for 1 h. After dissolving 5 mg of $C_6H_5Na_3O_7$ (worked as capping and reduction agent) in the dispersion, 5 mL of $Bi(NO_3)_3 \cdot 5H_2O$ in ethylene glycol was added and the mixture was stirred for 12 h. Then 0.5 mL of 0.1 M $NaBH_4$ was added to the mixture for reducing Bi^{3+}.[9–11] After shaking for 1 h, the synthesized solid products were separated by centrifugation, and then washed thoroughly with distilled water and absolute ethanol to remove any impurities. The obtained solid products were dried in a vacuum oven at 50 °C for 24 h. Finally, the BiNPs@$CoFe_2O_4$ nanocomposites were obtained.

2.4 Fabrication of BiNPs@$CoFe_2O_4$/GCE sensor

Before fabrication of sensor, the GCE was mechanically polished to a mirror-like surface with alumina micro powder (0.3 and 0.05 μm alumina slurries), successively sonicated with absolute ethanol, HNO_3 (0.05 M) and distilled water, respectively. After that, the GCE was activated in 0.5 M H_2SO_4.

1 mg BiNPs@$CoFe_2O_4$ nanocomposites were dispersed in 1 mL 0.20% CS solution and then sonicated to obtain homogeneous suspension. Then, 5 μL of the suspension was directly drop-cast on the pretreated GCE and dried in air. Finally, the BiNPs@$CoFe_2O_4$/GCE sensor was obtained.

2.5 Characterization

The morphology of $CoFe_2O_4$ porous microspheres and BiNPs@$CoFe_2O_4$ nanocomposites was characterized by SEM (NanoSEM45011, FEI, America) and TEM (JEM-2100, JEOL Inc., Japan). The elemental compositions were taken on EDX (EDAX Inc., Mahwah, USA). The crystallinity was determined by XRD diffractometer (D8 Advance, Bruker, karlsruhe, Germany). The chemical state of the samples was demonstrated using XPS (Da Vinci, Bruker, Germany).

2.6 Electrochemical measurements

Electrochemical measurements were performed on CHI660 electrochemical workstation (Shanghai Chenhua, China) and a conventional three-electrode system (counter electrode – platinum wire, working electrode – BiNPs@$CoFe_2O_4$/GCE, reference electrode – saturated calomel electrode (SCE)). The tested electrochemical techniques were cyclic voltammograms (CV), electrochemical impedance spectra (EIS) and chronocoulometry (CC). The electrochemical properties of the produced sensor were determined according to previous study. The active area of BiNPs@$CoFe_2O_4$ nanocomposites was calculated using the following equation:

$$Q(t) = \frac{2nFAcD^{1/2}t^{1/2}}{\pi^{1/2}} + Q_{dl} + Q_{ads}$$

where Q, the absolute value of the reduction charge; n, the number of electrons transfer; F, the Faraday constant (96 485 C mol^{-1}); A, the effective area; c, the substrate concentration; D, the diffusion coefficient (7.6×10^{-6} cm^2 s^{-1}); t, the time; Q_{dl}, the double-layer charge; Q_{ads}, the faradaic charge consumed by adsorbed species.

2.7 Electrochemical detection of Pb^{2+} and Cd^{2+}

SWASV was applied at a deposition potential of −1.1 V for 300 s in 0.1 M acetate buffer solution (pH 5.0), and performed in the potential range of −0.95 to −0.35 V with a frequency of 15 Hz, an amplitude of 25 mV, and an increment potential of 4 mV. The stability of BiNPs@$CoFe_2O_4$/GCE was investigated by repetitively determining 0.2 μM Pb^{2+} and 0.4 μM Cd^{2+} ten times and the response sensitivity was evaluated over six weeks. The reproducibility of the sensor was investigated by studying six sensors in parallel by detecting 0.2 μM Pb^{2+} and 0.4 μM Cd^{2+}.

3. Results and discussion

3.1 Characterization of the BiNPs@$CoFe_2O_4$

The porous spherical morphology and microstructure of $CoFe_2O_4$ were characterized by SEM. As shown in Fig. 1A, the diameter of $CoFe_2O_4$ was about 2 μm and the microspheres are uniform and homogenously dispersed. The high-magnification SEM image (Fig. 1B) indicated that its morphology resembles a dandelion pollen grain and exhibits a highly layered porous structure. The large pores on the outer wall of the microspheres are about 200 nm. $CoFe_2O_4$ was obviously porous and possessed a relatively large space inside the microspheres.[12] According to the previous report, a morphological evolution from nanoparticle aggregates to hierarchical porous $CoFe_2O_4$ structures. In the first stage of the synthesis reaction, at low pH values, Fe^{3+} can easily react with the OH^- produced by urea and NH_4F to form FeOOH and thus the nanoparticle aggregates were generated. Subsequent growth was took place around the grain boundary of the nanoparticle aggregates. With the reaction time increased, the FeOOH nanoparticle gradually dissolved and the dissolved Fe^{3+} combined with Co^{2+} can recrystallize into nanoparticles to form hierarchical $CoFe_2O_4$ porous microspheres. In this process, FeOOH nanoparticle worked as the template for porous structure. To further investigate the microstructure of BiNPs@$CoFe_2O_4$, TEM examination was conducted and the resulted picture indicated that the inner part of the microspheres is loose with large interspace (Fig. 1C), and the BiNPs (dark dots) were distributed on the $CoFe_2O_4$ microspheres hole surface and interior. The fringes of the marked lattice spacing

of 0.32 nm in Fig. 1D correspond to the (012) facet of Bi.[13] EDX mapping analysis (Fig. 1E and F) revealed that the Bi element was uniformly distributed on the microspheres, which confirmed the uniform and successful attachment of BiNPs on $CoFe_2O_4$.

As shown in Fig. 2A, all diffraction peaks of the XRD patterns can be assigned to a single phase of $CoFe_2O_4$ and Bi with a face-centered-cubic spinel structure (JCPDS no. 22-1086 and no. 5-519). For XPS spectrum (Fig. 2B), it is show that both $CoFe_2O_4$ microspheres and BiNPs@$CoFe_2O_4$ were composed Fe, Co, C, and O. Moreover, the XPS spectra of BiNPs@$CoFe_2O_4$ showed presence of Bi, suggesting that BiNPs@$CoFe_2O_4$ had been synthesized successfully. As shown in Fig. 2C, the peaks of Bi 4f ($4f_{7/2}$ and $4f_{5/2}$) were qualified to Bi(0), which indicated that nearly all bismuth in the BiNPs@$CoFe_2O_4$ was Bi(0).[14] In brief, all these results confirmed the successful preparation of BiNPs@$CoFe_2O_4$.

3.2 Electrochemical characterization of the BiNPs@$CoFe_2O_4$/GCE

The cyclic voltammograms in 5 mM $K_3[Fe(CN)_6]$ and 0.1 M KCl mixture solution were used to investigate the electron transfer properties of the electrodes. Comparing the cyclic voltammograms of bare GCE, $CoFe_2O_4$/GCE and BiNPs@$CoFe_2O_4$/GCE, it can be seen that BiNPs@$CoFe_2O_4$/GCE shows the largest peak current and the increase of peak current (Fig. 3A), indicating that the material of the modified electrode has good conductivity.[15] It is beneficial for $Fe(CN)_6^{3-/4-}$ to be close to the electrode surface. In addition, EIS was used to study the interfacial electron transfer resistance (Ret). The data in Fig. 3B showed that three Rets of 1500 U on bare GCE, 500 U of $CoFe_2O_4$/GCE and 100 U of BiNPs@$CoFe_2O_4$/GCE were obtained respectively. The reduced Ret was attributed to the distended high electrical conductivity and specific area, which can improve the transfer

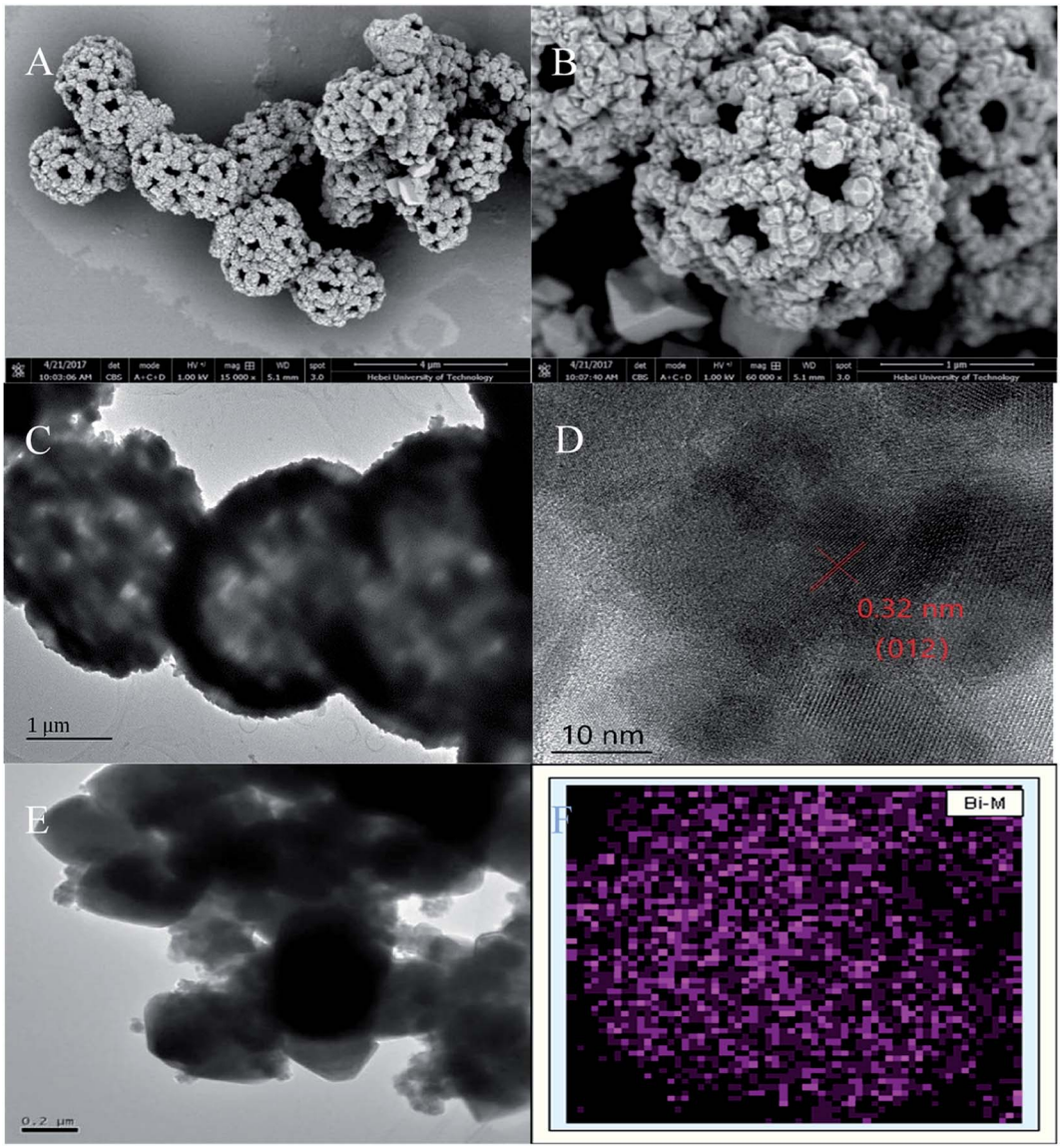

Fig. 1 (A and B) SEM images of $CoFe_2O_4$, (C and D) TEM images of $CoFe_2O_4$ and BiNPs@$CoFe_2O_4$, (E and F) EDX mapping of Bi.

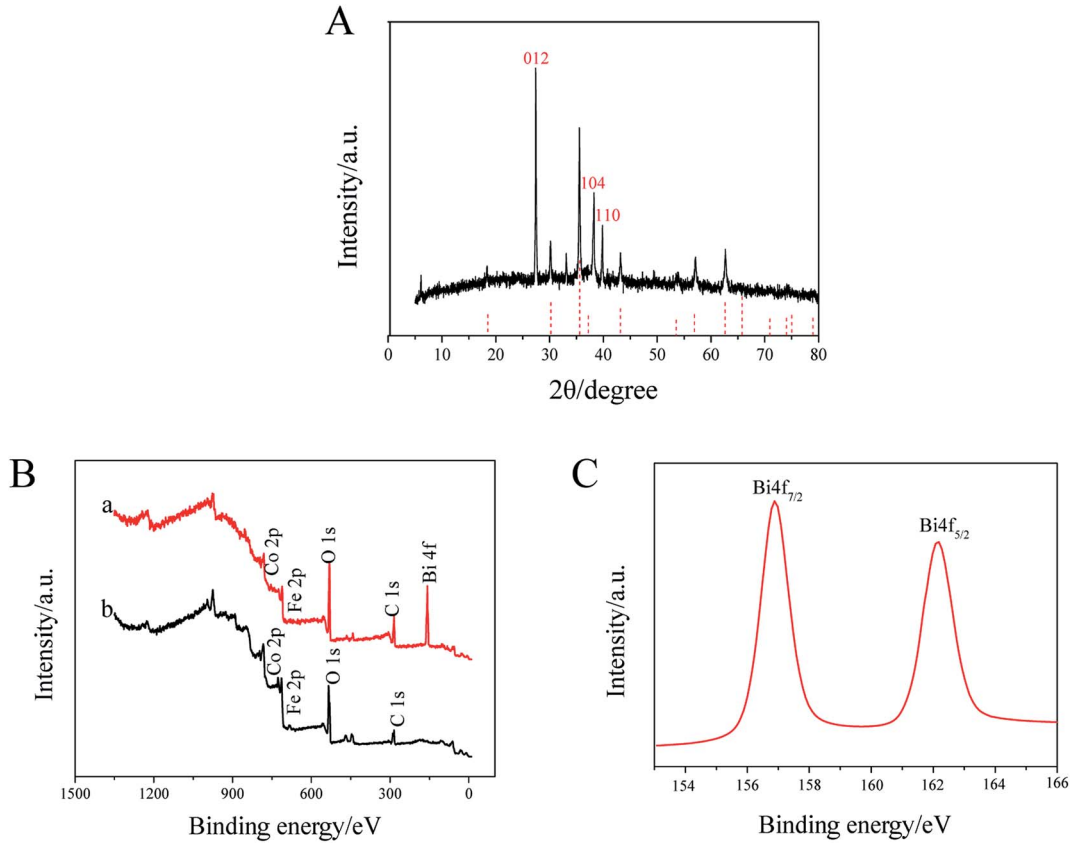

Fig. 2 (A) XRD pattern of BiNPs@$CoFe_2O_4$. (B) XPS spectra of $CoFe_2O_4$ (b) and BiNPs@$CoFe_2O_4$ (a), (C) Bi 4f XPS spectrum of Bi.

of electron and mass exchange of electro-active indicators on surface.[16] As shown in Fig. 3C and D, the active area of BiNPs@$CoFe_2O_4$/GCE is the largest (0.05315 cm^2) after calculation, indicating that it has a large electrode active area and can be used as a platform for sensitive sensing metal ions.[17] The above advantages can also be further demonstrated by the SWASV response to heavy metal ions. As shown in Fig. 4, we can observe sharp elution peaks and large peak currents, indicating that BiNPs@$CoFe_2O_4$/GCE has a good adsorption performance and electrical conductivity.

3.3 Optimization of working conditions for BiNPs@$CoFe_2O_4$/GCE

To optimize the sensitivity and accuracy of the modified electrode, the following parameters affecting electrode performance were optimized. Firstly, as shown in Fig. 5A, the Pb^{2+} and Cd^{2+} showed the optimum response current at pH 5.0. As shown in Fig. 5B, the deposition potential was also optimized. Obviously, the stripping voltammetric peak current of Pb^{2+} and Cd^{2+} reaches a maximum at −1.1 V. While further decreasing potentials, competitive hydrogen evolution was increased and led to the stripping voltammetric peak current of Pb^{2+} and Cd^{2+} are continuously decrease. Thus, −1.1 V was chosen as the optimal enrichment potential. Furthermore, deposition time was also optimized, as shown in Fig. 5C. It can be seen from the figure that the response signals increased rapidly due to more metal ions were reduced on the electrode. Next, the deposition time was increased to 500 s, slow increments in signals occurred due to the saturation of active sites on BiNPs. In practical applications, a higher response signal produced with shorter deposition time was favorable. Thus, in the following experiments, the deposition time of 300 s was chosen. The influence of mass fraction on response signals is shown in Fig. 5D. With increasing weight ratio of $CoFe_2O_4$, the SWASV responses of both Pb^{2+} and Cd^{2+} increased and reached maxima at 1 : 8. After reaching certain content, the SWASV peak currents of Pb^{2+} and Cd^{2+} begin to decrease, which could be attributed to the relatively low ratio of BiNPs.[18]

3.4 Analytical performance

As shown in Fig. 6A, the dissolution peak voltammetric potential of Pb^{2+} and Cd^{2+} on BiNPs@$CoFe_2O_4$/GCE are around −0.6 V and −0.8 V. With the increasing concentrations of Pb^{2+} and Cd^{2+}, the stripping peak currents exhibited a rapid and sensitive current response. The linear functional relationship between the amperometric response and the concentration was divided into two ranges, 0.06 to 0.6 μM and 0.08 to 0.8 μM, respectively. The linear equations were evaluated as $I/\mu A = -0.89174 + 49.97671C/\mu M$ and $I/\mu A = -2.55857 + 42.70202C/\mu M$ for Pb^{2+} and Cd^{2+}, with correlation coefficients of 0.99681

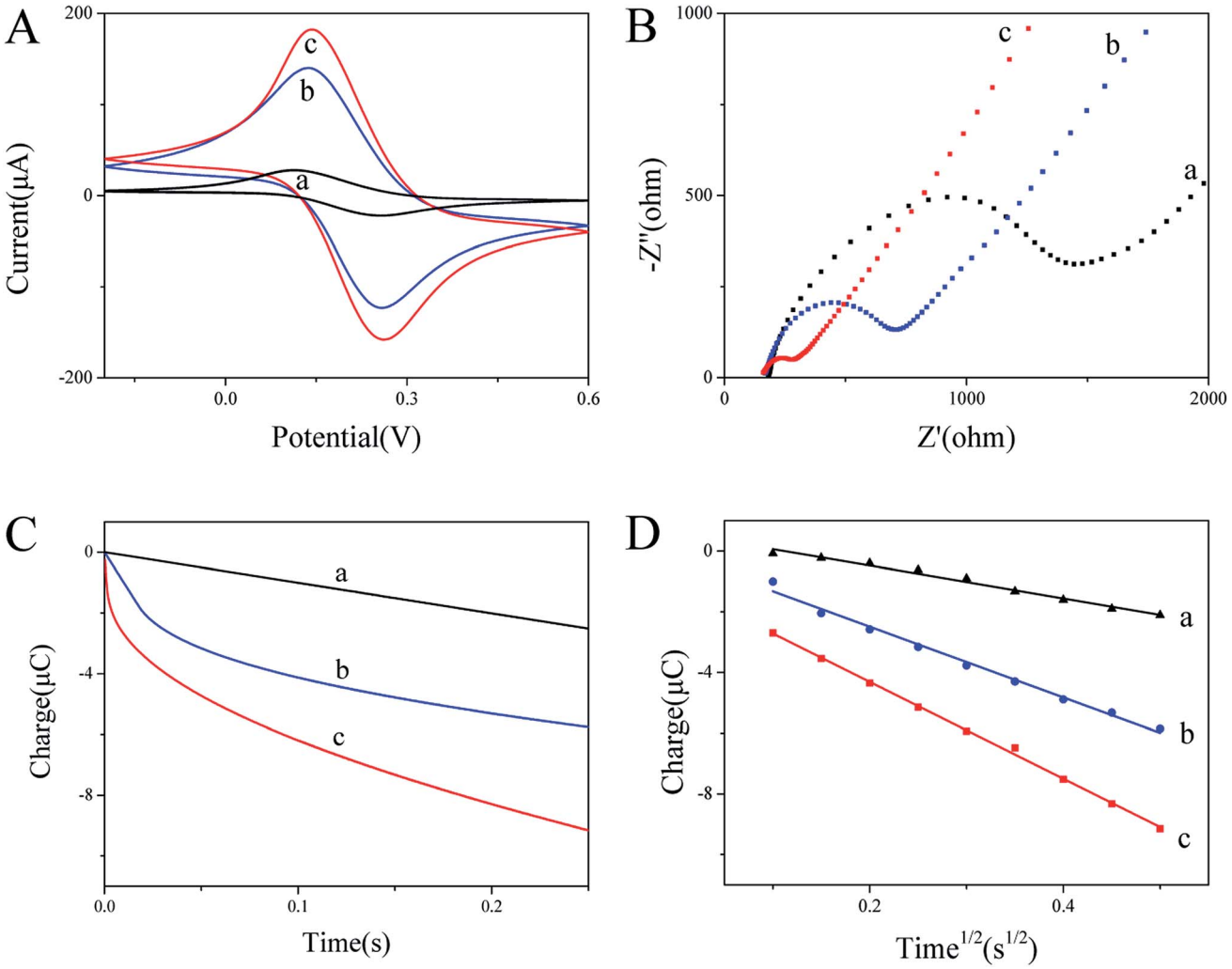

Fig. 3 (A) Cyclic voltammograms of GCE bare (a), $CoFe_2O_4$/GCE (b) and BiNPs@$CoFe_2O_4$/GCE (c); (B) EIS spectra of GCE bare (a), $CoFe_2O_4$/GCE (b) and BiNPs@$CoFe_2O_4$/GCE (c); (C and D) plots of $Q-t$ and $Q-t^{1/2}$ of the tested electrodes.

and 0.99333, respectively. The limits of detection were calculated to be 7.3 nM (1.51 ppb) for Pb^{2+} and 8.2 nM (0.92 ppb) for Cd^{2+}, which are much lower than the respective concentrations 10 μg L^{-1} and 3 μg L^{-1} specified by the World Health Organization.[19]

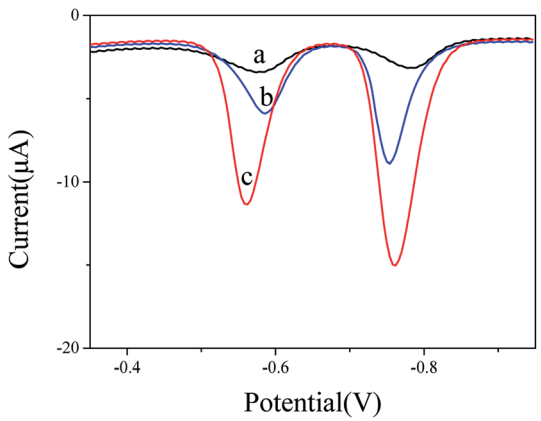

Fig. 4 SWASV curves of 0.2 μM Pb^{2+} and 0.4 μM Cd^{2+} at bare GCE (a), $CoFe_2O_4$/GCE (b) and BiNPs@$CoFe_2O_4$/GCE (c) in 0.1 M acetate buffer solution (pH 5.0).

3.5 Interference study

Mutual interference between heavy metal ions becomes a major problem in simultaneously detecting metal ions.[20] Therefore, the interference of Pb^{2+} and Cd^{2+} was evaluated. By keeping one ion concentration constant and increasing another ion concentration, the dissolution peak currents of the two are substantially unchanged. Furthermore, a good linear relationship between Pb^{2+} and Cd^{2+} are obtained in the ranges of 0.06–0.6 μM and 0.08–0.6 μM, respectively. The linear equations were evaluated as $I/\mu A = -1.40265 + 50.99795C/\mu M$ and $I/\mu A = -1.57632 + 38.80912C/\mu M$, for Pb^{2+} and Cd^{2+}, with correlation coefficients of 0.99499 and 0.99869, respectively. The detection slopes of both Pb^{2+} and Cd^{2+} were similar to those shown in Fig. 7 (50.99795 and 49.97671 for Pb^{2+} and 38.80912 and 42.70202 for Cd^{2+}), which indicated that no mutual interference between Pb^{2+} and Cd^{2+} at BiNPs@$CoFe_2O_4$/GCE.

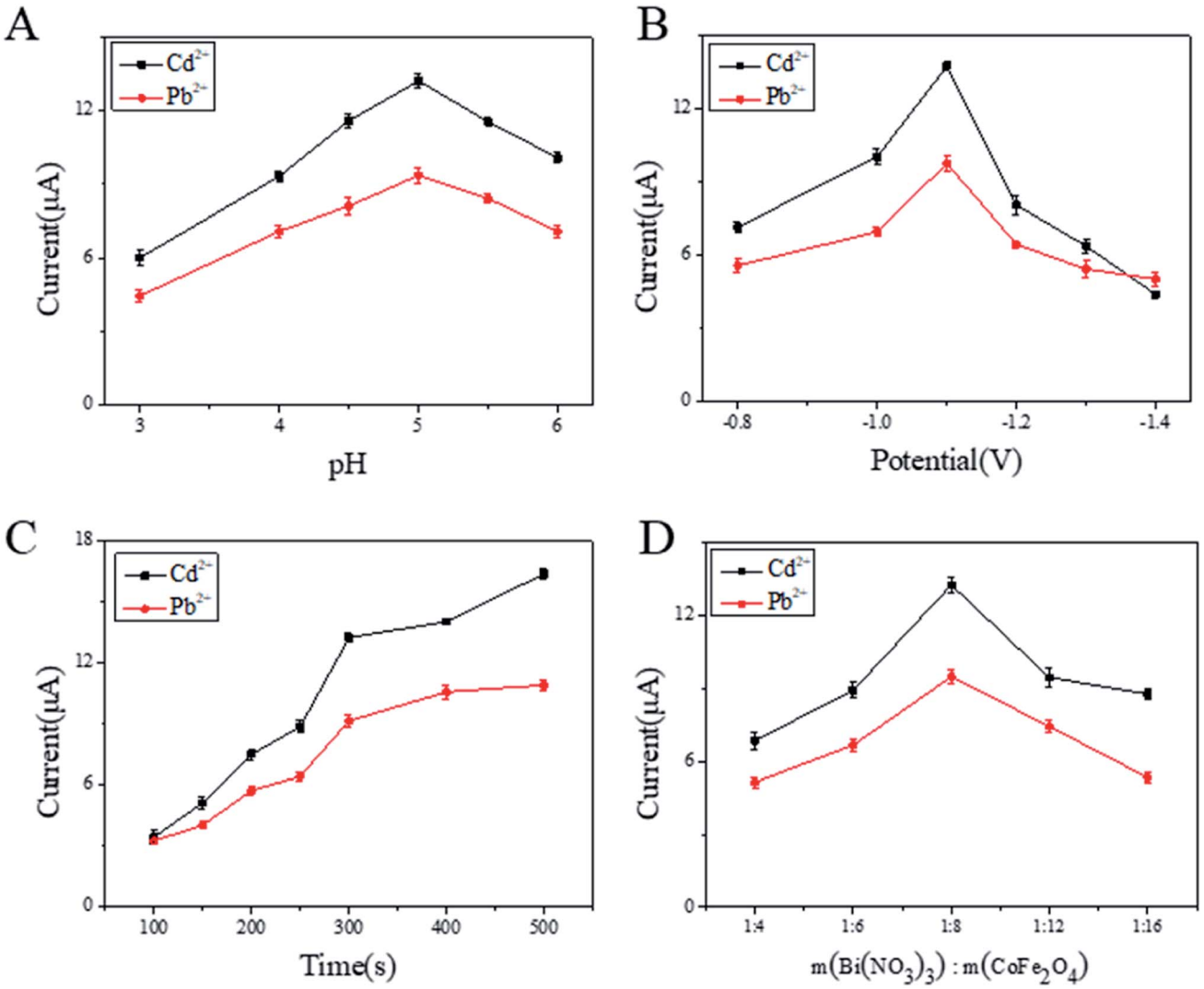

Fig. 5 Optimization of experimental conditions (A–D) on SWASV response of 0.2 μM Pb^{2+} and 0.4 μM Cd^{2+} in acetate buffer at BiNPs@$CoFe_2O_4$/GCE.

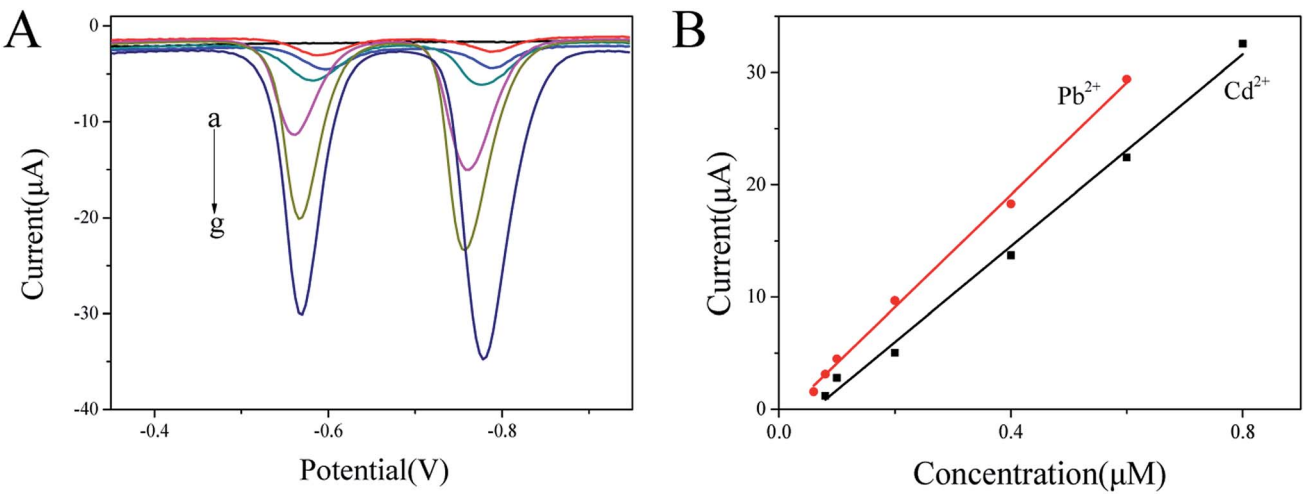

Fig. 6 (A) SWASV responses of BiNPs@$CoFe_2O_4$/GCE for the simultaneous analysis of Pb^{2+} and Cd^{2+} at 0, 0.06, 0.08, 0.1, 0.2, 0.4 and 0.6 μM for Pb^{2+}, and 0, 0.08, 0.1, 0.2, 0.4, 0.6 and 0.8 μM Cd^{2+}, respectively. (B) Calibration curves for Pb^{2+} and Cd^{2+}.

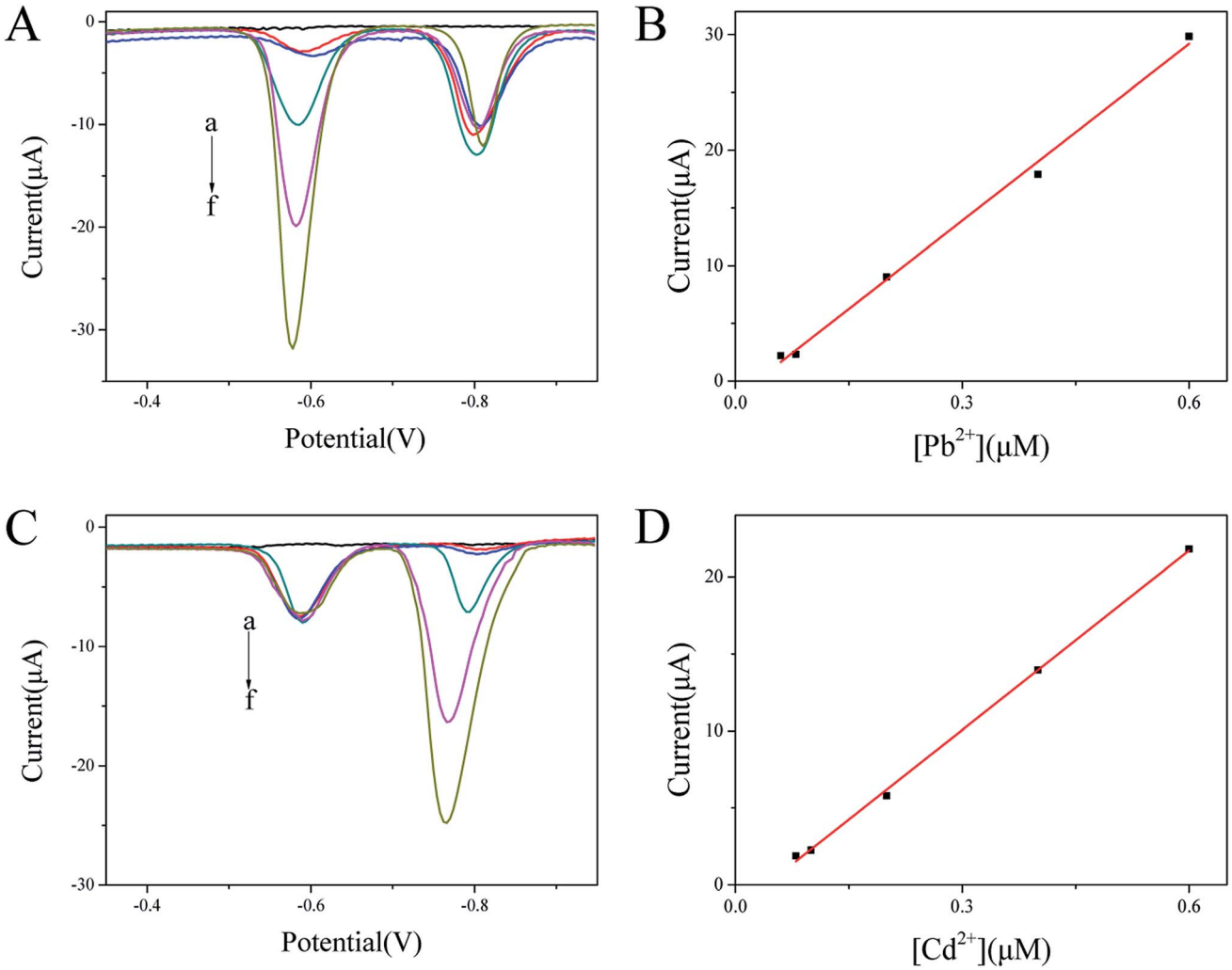

Fig. 7 (A) SWASV curves of Pb^{2+} at 0, 0.06, 0.08, 0.2, 0.4 and 0.6 μM in presence of 0.4 μM Cd^{2+} at BiNPs@$CoFe_2O_4$/GCE. (B) Corresponding linear calibration plots against Pb^{2+}. (C) SWASV curves of Cd^{2+} at 0, 0.08, 0.1, 0.2, 0.4 and 0.6 μM in presence of 0.2 μM Pb^{2+} at BiNPs@$CoFe_2O_4$/GCE. (D) Corresponding linear calibration plots against Cd^{2+}.

In order to explore the anti-interference performance of this sensor, interfering ions such as Mg^{2+}, Al^{3+}, Cu^{2+}, Zn^{2+}, Mn^{2+}, Co^{2+}, Ni^{2+} and Fe^{3+} were added to 0.2 μM Pb^{2+} and 0.4 μM Cd^{2+} at a concentration of 10 μM. The results in Fig. 8 show little changes in response signals except Cu^{2+}. In the state of adding Cu^{2+}, the signals were significantly reduced, which may be due to the intermetallic compounds formation that can be avoided by adding ferrocyanide for forming Cu^{2+} stable complexes.[21] In addition, the anions such as Cl^-, SO_4^{2-} and NO_3^- did not have obvious effect on the stripping peak current. The results demonstrated that the prepared the sensor had anti-interference ability.

3.6 Reproducibility and stability of the sensors

Reproducibility and long-term stability are important parameters to evaluate the performance of the sensors. The repeatability of the BiNPs@$CoFe_2O_4$/GCE was performed by stripping voltammetry of 0.2 μM Pb^{2+} and 0.4 μM Cd^{2+} ten times. The relative standard deviation (RSD) was found to be 3.2% and 2.5%. These results indicated that the BiNPs@$CoFe_2O_4$/GCE sensors possessed excellent stability. When it was stored six weeks, the sensor remained about 94% and 93% of its original

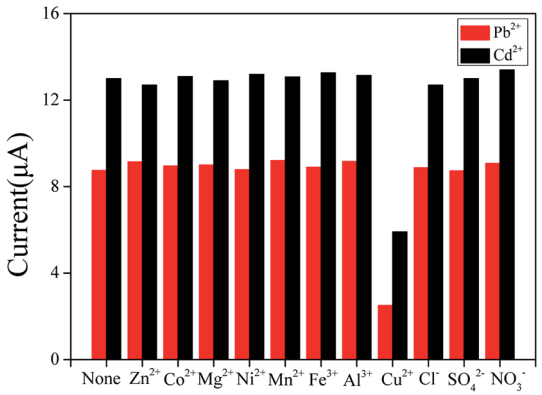

Fig. 8 Selectivity of BiNPs@$CoFe_2O_4$/GCE for simultaneous detection of Pb^{2+} and Cd^{2+}.

Table 1 Determination of Pb^{2+} and Cd^{2+} in water samples with the BiNPs@$CoFe_2O_4$/GCE

Samples	Added (nM)	Result (nM)	Recovery (%)
Tap water	Pb^{2+} 150	148.3 ± 1.05	98.9
	Cd^{2+} 150	155.4 ± 1.31	103.6

response for Pb^{2+} and Cd^{2+}, respectively. The reproducibility of six electrodes which were prepared in parallel with the same modification method was also studied. The corresponding relative standard deviations of detecting 0.2 μM Pb^{2+} and 0.4 μM Cd^{2+} were 3.7% and 2.7%, respectively. The high stability and good reproducibility was recognized to the structure stability nature and binding strength of BiNPs@$CoFe_2O_4$ nanocomposites on GCE.[22]

3.7 Practical assay in tap water

Recovery experiments were used to demonstrate the applicability of the sensors in tap water samples. The concentrations of Pb^{2+} and Cd^{2+} were calculated through the standard addition method, with additions of 150 nM Pb^{2+} and 150 nM Cd^{2+}. As shown in Table 1, the recovery rate of Pb^{2+} and Cd^{2+} are 98.9% ∼ 103.6%. The above results show that the sensors can be used for the detection of Pb^{2+} and Cd^{2+} in real samples.

As can be seen in Table 2, the detection limits of BiNPs@$CoFe_2O_4$/GCE were compared with the reported electrodes modified with other materials. The detection limit of Cd^{2+} is obviously lower than that of most other modified electrodes, but the detection limit of Pb^{2+} is not ideal, which may be due to that BiNPs@$CoFe_2O_4$ nanocomposites integrated the advantages of BiNPs and $CoFe_2O_4$ including high surface area and good conductivity. Therefore, the BiNPs@$CoFe_2O_4$ nanocomposites can be applied as a good electrode-modification material for fast and convenient determining of heavy metal ions in environmental systems.

Table 2 List of various electrochemical sensors for Pb^{2+} and Cd^{2+} detection

Electrochemical platform	Technique	Analyte (HMI)	LOD
Bi–C nanocomposite[23]	SWASV	Pb^{2+}	0.65 ppb
		Cd^{2+}	0.81 ppb
RGO/Bi nanocomposite[24]	ASV	Pb^{2+}	0.55 ppb
		Cd^{2+}	2.8 ppb
BiNPs[25]	SWASV	Pb^{2+}	2 ppb
		Cd^{2+}	5 ppb
Nano-Bi[26]	SWASV	Pb^{2+}	1.97 ppb
		Cd^{2+}	2.54 ppb
NPCGS/Bi nanocomposite[18]	SWASV	Pb^{2+}	0.66 ppb
		Cd^{2+}	0.46 ppb
$CoFe_2O_4$/Bi nanocomposite	SWASV	Pb^{2+}	1.51 ppb
		Cd^{2+}	0.92 ppb

4. Conclusions

Through combining the advantages of BiNPs and $CoFe_2O_4$, BiNPs@$CoFe_2O_4$ nanocomposites with high surface area and good conductivity were prepared. BiNPs@$CoFe_2O_4$ was used to modify electrochemical electrode for heavy metal ions detection as sensing technology. The obtained sensor can simultaneously detect Pb^{2+} and Cd^{2+} with high sensitivity and good exactness. Thus, the BiNPs@$CoFe_2O_4$ nanocomposites can be applied as an excellent electrode-modification material for fast and convenient determining of heavy metal ions in environmental systems.

Conflicts of interest

There are no conflicts to declare.

References

1 P. B. Tchounwou, C. G. Yedjou, A. K. Patlolla and D. J. Sutton, Heavy Metal Toxicity and the Environment, *Molecular, Clinical and Environmental Toxicology*, 2012, **101**, 133–164.
2 A. Afkhami, F. S. Felehgari, T. Madrakian, H. Ghaedi and M. Rezaeivala, Fabrication and application of a new modified electrochemical sensor using nano-silica and a newly synthesized Schiff base for simultaneous determination of Cd^{2+}, Cu^{2+} and Hg^{2+} ions in water and some foodstuff samples, *Anal. Chim. Acta*, 2013, **771**, 21–30.
3 T. Gong, J. Liu, X. Liu, J. Liu, J. Xiang and Y. Wu, A sensitive and selective platform based on CdTe QDs in the presence of L-cysteine for detection of silver, mercury and copper ions in water and various drinks, *Food Chem.*, 2016, **213**, 306–312.
4 L. Pujol, D. Evrard, K. G. Serrano, M. Freyssinier, A. R. Cizsak and P. Gros, Electrochemical sensors and devices for heavy metals assay in water: the French groups' contribution, *Front. Chem.*, 2014, **2**, 19.
5 G. Aragay and A. Merkoci, Nanomaterials application in electrochemical detection of heavy metals, *Electrochim. Acta*, 2012, **84**, 49–61.
6 N. Serrano, A. Alberich, J. M. D. Cruz, C. Arino and M. Esteban, Coating methods, modifiers and applications of bismuth screen-printed electrodes, *TrAC, Trends Anal. Chem.*, 2013, **46**, 15–29.
7 L. Zhao, H. Zhang, Y. Xing, S. Song, S. Yu, W. Shi, X. Guo, J. Yang, Y. Lei and F. Cao, Studies on the magnetism of cobalt ferrite nanocrystals synthesized by hydrothermal method, *J. Solid State Chem.*, 2008, **181**, 245–252.
8 A. S. Teja and P. Y. Koh, Synthesis, properties and applications of magnetic iron oxide nanoparticles, *Prog. Cryst. Growth Charact. Mater.*, 2009, **55**, 22–45.
9 C. Stubenrauch, T. Wielputz, T. Sottmann, C. Roychowdhury and F. J. Disalvo, Microemulsions as templates for the synthesis of metallic nanoparticles, *Colloids Surf., A*, 2008, **317**, 328–338.
10 X. Hu, D. Pan, H. Han, M. Lin, Y. Zhu and C. Wang, Preparation of bismuth-based microrods and their application in electroanalysis, *Mater. Lett.*, 2017, **190**, 83–85.

11 K. Chen, W. Fan, C. Huang and X. Qiu, Enhanced stability and catalytic activity of bismuth nanoparticles by modified with porous silica, *J. Phys. Chem. Solids*, 2017, **110**, 9–14.
12 I. Safarik and M. Safarikova, Magnetic nano- and microparticles in biotechnology, *Chem. Pap.*, 2009, **63**, 497–505.
13 P. Xiong, P. Bai, A. Li, B. Li, M. Cheng, Y. Chen, S. Huang, Q. Jiang, X. H. Bu and Y. Xu, Bismuth Nanoparticle@Carbon Composite Anodes for Ultralong Cycle Life and High-Rate Sodium-Ion Batteries, *Adv. Mater.*, 2019, **31**, 1904771.
14 L. Shi, Y. Li, X. Rong, Y. Wang and S. Ding, Facile fabrication of a novel 3D graphene framework/Bi nanoparticle film for ultrasensitive electrochemical assays of heavy metal ions, *Anal. Chim. Acta*, 2017, **968**, 21–29.
15 C. Shen, L. Wang, A. Zhou, B. Wang, X. Wang, W. Lian, Q. Hu, G. Qin and X. Liu, Synthesis and Electrochemical Properties of Two-Dimensional RGO/$Ti_3C_2T_x$ Nanocomposites, *Nanomaterials*, 2018, **8**, 80–88.
16 Y. Liu, W. Wang, Y. Ying, Y. Wang and X. Peng, Binder-free layered Ti_3C_2/CNTs nanocomposite anodes with enhanced capacity and long-cycle life for lithium-ion batteries, *Dalton Trans.*, 2015, **44**, 7123–7126.
17 Z. Wang, H. Guo, E. Liu, G. Yang and K. N. Win, Bismuth/Polyaniline/Glassy Carbon Electrodes Prepared with Different Protocols for Stripping Voltammetric Determination of Trace Cd and Pb in Solutions Having Surfactants, *Electroanalysis*, 2010, **22**, 209–215.
18 L. Cui, J. Wu and H. Ju, Synthesis of Bismuth-Nanoparticle-Enriched Nanoporous Carbon on Graphene for Efficient Electrochemical Analysis of Heavy-Metal Ions, *Chem.–Eur. J.*, 2015, **21**, 11525–11530.
19 M. B. Gumpu, S. Sethuraman, U. M. Krishnan and J. B. B. Rayappan, A review on detection of heavy metal ions in water – an electrochemical approach, *Sens. Actuators, B*, 2015, **213**, 515–533.
20 P. A. Dimovasilis and M. I. Prodromidis, Bismuth-dispersed xerogel-based composite films for trace Pb(II) and Cd(II) voltammetric determination, *Anal. Chim. Acta*, 2013, **769**, 49–55.
21 L. Cui, J. Wu and H. Ju, Electrochemical sensing of heavy metal ions with inorganic, organic and bio-materials, *Biosens. Bioelectron.*, 2015, **63**, 276–286.
22 S. Lee, S. Bong, J. Ha, M. Kwak, S. K. Park and Y. Piao, Electrochemical deposition of bismuth on activated graphene-nafion composite for anodic stripping voltammetric determination of trace heavy metals, *Sens. Actuators, B*, 2015, **215**, 62–69.
23 P. Niu, C. F. Sanchez, M. Gich, C. Ayora and A. Roig, Electroanalytical Assessment of Heavy Metals in Waters with Bismuth Nanoparticle-Porous Carbon Paste Electrodes, *Electrochim. Acta*, 2015, **165**, 155–161.
24 P. K. Sahoo, B. Panigrahy, S. Sahoo, A. K. Satpati, D. Li and D. Bahadur, *In situ* synthesis and properties of reduced graphene oxide/Bi nanocomposites: as an electroactive material for analysis of heavy metals, *Biosens. Bioelectron.*, 2013, **43**, 293–296.
25 M. Cadevall, J. Ros and A. Merkoci, Bismuth nanoparticles integration into heavy metal electrochemical stripping sensor, *Electrophoresis*, 2015, **36**, 1872–1879.
26 G. J. Lee, C. K. Kim, M. G. Lee and K. R. Chang, Simultaneous Voltammetric Determination of Zn, Cd and Pb at Bismuth Nanopowder Electrodes with Various Particle Size Distributions, *Electroanalysis*, 2010, **22**, 530–535.